Spatially Resolved Neutral Wind Response Times During High Geomagnetic Activity Above Svalbard

D. D. Billett[1], J. A. Wild[1], A. Grocott[1], A. L. Aruliah[2], A. M. Ronksley[2], M.-T. Walach[1], M. Lester[3]

[1]Physics Department, Lancaster University, Bailrigg, Lancaster, LA1 4YB, United Kingdom.
[2]Department of Physics and Astronomy, University College London, Gower Street, London, WC1E 6BT, United Kingdom.
[3]Department of Physics and Astronomy, University of Leicester, University Road, Leicester, LE1 7RH, United Kingdom.

Key Points:

- The delay of thermospheric neutral winds fully responding to changes in ion-drag is examined for locations separated by about 100 km
- In this study, neutrals took 67-97 minutes to fully change velocity after changes in the ionospheric plasma, for regions within a 1000 km FOV
- The neutral wind flywheel effect is significant when the neutral velocity begins to overtake that of the plasma

Corresponding author: D. D. Billett, `d.billet@lancaster.ac.uk`

Abstract

It has previously been shown that in the high latitude thermosphere, sudden changes in plasma velocity (such as those due to changes in interplanetary magnetic field) are not immediately propagated into the neutral gas via the ion-drag force. This is due to the neutral particles (O, O_2 and N_2) constituting the bulk mass of the thermospheric altitude range, and thus holding on to residual inertia from a previous level of geomagnetic forcing. This means that consistent forcing (or dragging) from the ionospheric plasma is required, over a period of time long enough, for the neutrals to reach an equilibrium with regards to ion-drag. Furthermore, mesoscale variations in the plasma convection morphology, solar pressure gradients and other forces indicate that the thermosphere-ionosphere coupling mechanism will also vary in strength across small spatial scales. Using data from the Super Dual Auroral Radar Network (SuperDARN) and a Scanning Doppler Imager (SCANDI), a geomagnetically active event was identified which showed plasma flows clearly imparting momentum to the neutrals. A cross-correlation analysis determined that the average time for the neutral winds to accelerate fully into the direction of ion-drag was 75 minutes, but crucially, this time varied by up to 30 minutes (between 67 and 97 minutes) within a 1000 km field of view at an altitude of around 250 km. It is clear from this that the mesoscale structure of both the plasma and neutrals have a significant effect on ion neutral coupling strength, and thus energy transfer in the thermosphere.

1 Introduction

The mechanisms by which the high latitude thermosphere and ionosphere are linked are not completely understood. The motion of ionospheric plasma is controlled primarily via electromagnetic coupling to the magnetosphere and solar wind (Dungey, 1961), but the neutral background is considerably more complicated. Globally, thermospheric dynamics are mainly governed by the diurnal tides of solar heating, but in the high and mid latitudes, Coriolis forces and collisions between the neutrals and plasma drive a complex system which means that the dynamics of neither can be described by a single process. During geomagnetically active times, upwelling from the lower atmosphere and strong wind shears (especially near the auroral zone) can also increase advection and viscous forces (Titheridge, 1995).

The main driver of dynamics in the Earth's polar ionosphere is the convection of plasma due to the opening and closing of flux in the dayside and nightside magnetosphere respectively (Cowley & Lockwood, 1992). This process is controlled by the magnitude and orientation of the interplanetary magnetic field (IMF), in particular the B_z and B_y components (Ruohoniemi & Baker, 1998). Reconfiguration of the ionospheric convection as a response to changes in these two components happens relatively quickly, on the order of tens of minutes depending on local time (Murr & Hughes, 2001) and time history of the IMF (e.g. Grocott and Milan (2014)). However, how the neutral thermosphere reacts to sudden changes in plasma velocity is not fully understood.

There are two major factors which contribute to the large scale neutral winds formed in the polar regions of Earth. The first is the day to night pressure gradient induced by solar irradiance creating a diurnal, high temperature "bulge" at approximately 14:00 solar local time (SLT) (Jacchia, 1965). This component is reasonably well understood, and produces a broadly anti-sunward flow across the polar cap from approximately 14:00 to 02:00 SLT (Kohl & King, 1967). The second major factor is the drag force imposed on the neutrals from plasma in the ionosphere. During geomagnetically-quiet times, such as when the IMF B_z component is positive, plasma motion above 65° geomagnetic latitude has relatively low velocities (~30-200 $\mathrm{ms^{-1}}$) (Cousins & Shepherd, 2010; Ruohoniemi & Greenwald, 2005; Thomas & Shepherd, 2018; Weimer, 2005). During geomagnetically-active periods, the high latitude plasma convection extends further equatorward and is characterised by greater velocities up to a few kilometers per second. Due to a more pronounced influence from ion-drag forcing, the neutral wind field morphology then begins to resemble that of the plasma convection. This behaviour has been explored in statistical studies involving satellite measurements (Förster, Rentz, Köhler, Liu, & Haaland, 2008; Richmond, Lathuillere, & Vennerstrøm, 2003) and ground based instruments (Emmert et al., 2006), but also in numerical models (Drob et al., 2015; Richmond, Ridley, & Roble, 1992). Although these specify the average morphology of the neutrals under specific conditions, how they respond to localised and sudden changes in plasma velocity is still unclear, especially during geomagnetically-active periods.

At thermospheric altitudes, neutral particles accelerate when momentum is exchanged between the plasma and the neutrals via collisions. However, the neutrals do not accelerate to the velocity of the plasma instantaneously (Killeen et al., 1984). This is because the neutral gas mass is much greater than the plasma mass at these altitudes, so in order for them to accelerate fully to the velocity of the plasma (assuming only ion-drag acts on them), they require consistent forcing. Therefore, upon a change in plasma velocity (e.g. because of changes in the IMF or a substorm event) a duration of time (or 'lag') will exist between the change in forcing and the velocity of the neutral particles reaching some equilibrium state (as a response to the change in the ion-drag force). This means that during an interval equal to the time lag, there will be greater momentum exchanged due to neutral-ion collisions, and thus increased Joule heating.

Estimates of how long the neutral wind takes to fully respond to a change in the plasma velocity vary significantly depending on geomagnetic conditions and local time, or even the analysis method used. For instance, one method involves defining the ion-neutral e-folding time in seconds, τ, from a simplified momentum equation neglecting all forces except ion-drag, after Baron and Wand (1983):

$$\tau = \frac{(\mathbf{V} - \mathbf{U})}{\delta \mathbf{U}/\delta t} \qquad (1)$$

where $\mathbf{V}$ and $\mathbf{U}$ are the plasma and neutral velocity vectors respectively. Studies using this method on individual events, however, produce a wide range of e-folding times due to typically rapid variations in plasma measurements. For instance, Kosch, Cierpka, Rietveld, Hagfors, and Schlegel (2001) used co-incident EISCAT incoherent scatter radar (ISR) ion measurements and Fabry-Perot Interferometer (FPI) neutral measurements over a near 7-hour time interval to calculate τ, which was found to vary between 30 and 300 minutes. More recently, Joshi et al. (2015) used mid-latitude SuperDARN radars and FPI instruments to calculate τ with values falling in the range of 10 to 360 minutes, also varying rapidly from measurement to measurement. This makes clear an issue when trying to determine a neutral wind lag time from plasma or neutrals with high temporal variability; sudden increases or decreases in plasma velocity which are not sustained will mean that the neutrals do not have enough time to respond, and thus never fully accelerate or decelerate to some equilibrium state.

Joshi et al. (2015) also presented a different method for determining neutral lag time. This comprised a relatively simple cross-correlation analysis whereby a time series of neutral measurements was lagged back at constant time steps to the beginning of the plasma measurements, with a correlation coefficient calculated at each lag. In this technique, the lag when the neutrals are most correlated with the plasma is taken to be the delay of the neutrals. In the storm-time example event shown by Joshi et al. (2015), plasma and neutral velocities are relatively small due to being at sub-auroral latitudes, but a peak in the cross-correlation analysis was found at a lag of 84 minutes behind the plasma. This implies that ion-neutral coupling can be a critical driver of the neutrals, even at latitudes that are close to the equatorward boundary of convection.

Recently, Conde, Bristow, Hampton, and Elliott (2018) reported that during intervals of enhanced auroral activity, forcing via ion-drag has a significant effect on horizontal neutral winds over temporal and spatial scales much shorter than originally thought, on the order of 15 minutes and hundreds of kilometers. This is understood to be due to the increased ionisation brought about from particle precipitation, increasing ion-neutral collision frequencies, and thus coupling. Similar observations were also made by Zou et al. (2018). Both of these studies exploited results from a Scanning Doppler Imager (SDI), a type of FPI which can measure more than one single point neutral wind measurement (Conde & Smith, 1997), setting it apart from traditional FPIs. In this study we utilize SCANDI (Aruliah, Griffin, Yiu, McWhirter, & Charalambous, 2010), a similar class of instrument and in this case located on Spitsbergen, Svalbard (75.8°N, 108.7°E altitude adjusted corrected geomagnetic coordinates (AACGM) (Shepherd, 2014) as of 2018). It should be noted that all previous studies mentioned (apart from those so far in this paragraph) have focused on determining a single neutral wind lag time over their respective thermospheric fields-of-view. SCANDI allows a neutral wind delay to changes in the plasma to be resolved for each neutral wind vector determined, at a spatial resolution of approximately 100 km at 250 km altitude, thus allowing the examination of mesoscale changes in ion-drag. In this study, we achieve this by preforming a cross-correlation analysis with data from the Super Dual Auroral Radar Network (SuperDARN). It should be noted that the thermosphere above Svalbard is typically poleward of the auroral oval during active geomagnetic periods (e.g. Eather and Mende (1971)). Thus, we would usually expect the neutral velocities observed by SCANDI to have longer lag times than those found by Conde et al. (2018) and Zou et al. (2018) due to less ionisation from increased particle precipitation, resulting in fewer collisions between the plasma and neutrals. In the following sections, we describe the instruments used in more detail, as well as the event chosen. In the observations and discussion section, we detail a cross-correlation analysis of the respective data and derive spatially resolved neutral wind lag times with respect to changes in the plasma velocity for this event.

2 Data

2.1 SuperDARN

The Super Dual Auroral Radar Network (SuperDARN) consists of 35 high-frequency coherent scatter radars offering near total coverage of the high-latitude northern and southern hemisphere ionosphere (Chisham et al., 2007). The line of sight velocity of ionospheric irregularities in the field of view of each radar can be inferred from the Doppler shifts of backscattered signals. When multiple radars overlook the same region and receive backscatter, a true horizontal vector of the convective plasma may be obtained. More commonly, line of sight data are combined from all radars in the same hemisphere. An empirical model then contributes additional flow vectors that constrains a spherical harmonic fit in regions of poor data coverage. The result is a hemispheric map of the full, instantaneous convection pattern. Several different empirical models exist for this process and are typically dependent on the data coverage at the time of creation. For instance, Ruohoniemi and Greenwald (1996) used a single radar located in Canada to generate statistical patterns of the high latitude convection based on a 6-year interval of data. More recently however, newer models have fully utilized the global extent of SuperDARN and more complete historical data from all available radars, including newer radars which are located at mid-latitudes (Thomas & Shepherd, 2018). For this study, we used data from all available SuperDARN radars and the most recent electrostatic potential fitting model from Thomas and Shepherd (2018) to obtain plasma velocity measurements at an altitude of approximately 250 km, using the technique described by Ruohoniemi and Baker (1998). We also ensured that for the times and positions of interest, there was nearly always backscatter data from both radars overlooking SCANDI so that the model-stabilised flow estimates were well constrained (these are the radars located at Hankasalmi, Finland and Pykkvibaer, Iceland, as shown in Figure 1). An additional check was made to make sure that the fitted vectors used in this study were data driven, as opposed to being driven by the statistical model. If the latter were true, then changes in the plasma velocity due to changing IMF conditions could be solely due to the model switching between different model bins (which are dependent on IMF orientation and magnitude). Fitted velocities were derived using a static IMF model run using the same data, and compared against those generated using the dynamic model. No significant differences were found, likely as a result of radar backscatter coverage having been good throughout the event.

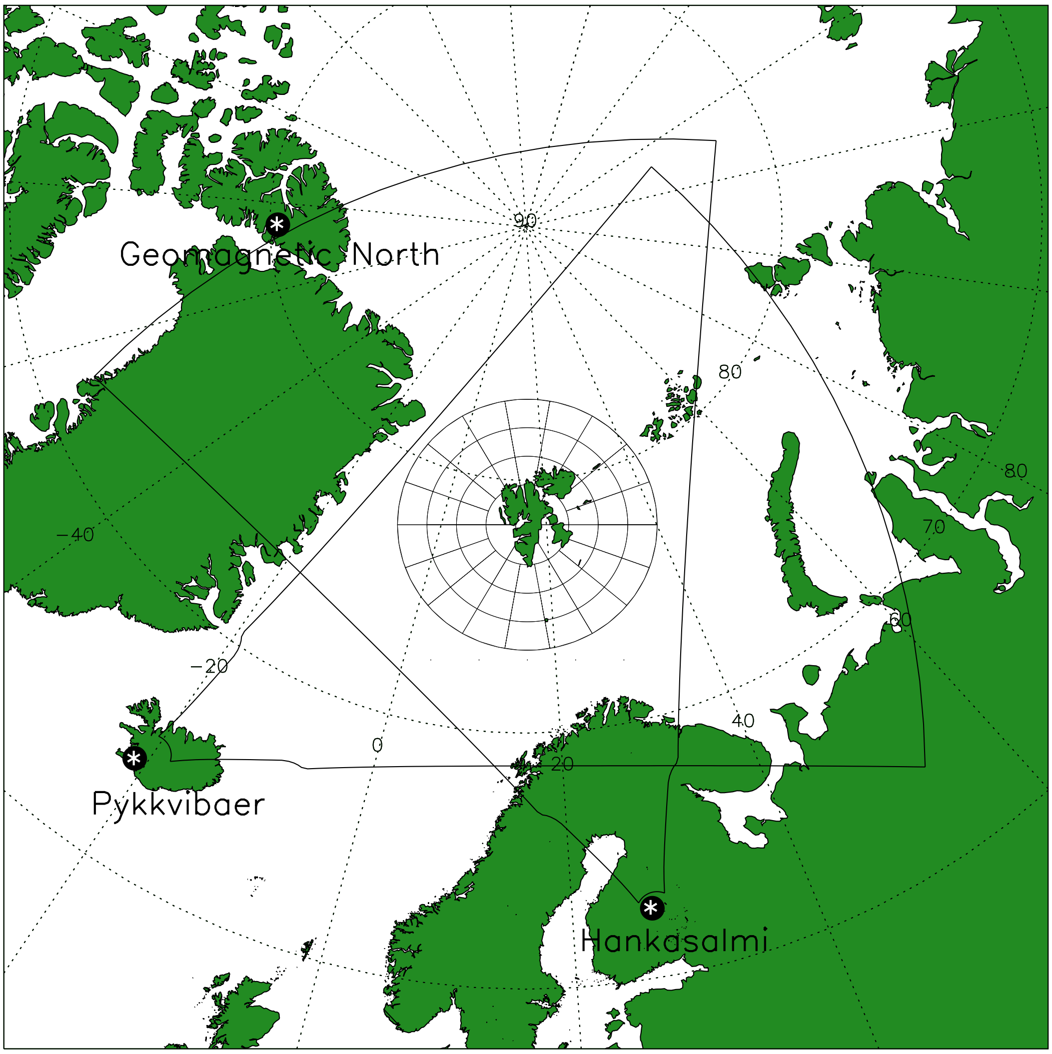

Figure 1. The configuration of SCANDI zones above Svalbard presented in stereographic geographic coordinates. Also shown are the fields of view of both overlapping SuperDARN radars and the location of the geomagnetic north pole (as of 2018). The fields of view of both SCANDI and SuperDARN radars are mapped to 250 km altitude.

2.2 SCANDI

SCANDI can measure multiple neutral wind vectors in an approximately 1000 km diameter field of view above Svalbard. This is achieved by measuring the Doppler shifts and broadening of auroral emissions and airglow, from which winds are calculated. Details of the procedure and sources of error can be found in Aruliah et al. (2010), after Conde and Smith (1998). Generally, the uncertainty in a given line-of-sight wind is determined by the brightness of the emission. Dark skies (solar zenith angle greater than

6 deg) are required to ensure a good signal to noise ratio (>300). Cloud-free skies are also required, as cloud scatters light from other parts of the sky and contaminates the Doppler profile of the line-of-sight emission. During geomagnetically active conditions within the auroral region, small inconsistencies can also sometimes be seen in the flows between neighbouring vector measurements. These are likely due to the assumption in vector derivation that the vertical wind is negligable, which is less true when the thermosphere is significantly disturbed (Kurihara et al., 2009). Vertical winds are however difficult to estimate from a single FPI without introducing further errors.

Emission spectra from SCANDI are subdivided into zones and a wind vector derived in each. For this study, a 61 zone configuration is used, offering an approximate 100 km spatial resolution. Figure 1 shows this configuration on a polar plot in geographic coordinates. Also shown are the fields of view of the two overlapping SuperDARN radars and the geomagnetic north pole as of 2018.

3 Observations

An event was found which occurred on the 8th December, 2013 that appeared to show considerably large signatures of ion-neutral coupling. Figure 2 presents an overview of this event, including the IMF B_z and $B_y$components (panel a), as well as the plasma and neutral velocity magnitudes averaged over all 61 SCANDI zones (panel b). The time integration of SCANDI is approximately 7.5 minutes, whilst the SuperDARN data has a two-minute integration. MLT-MLAT format plots showing both SuperDARN and SCANDI data for the times t_1, t_2, t_3 and t_4 indicated by vertical dashed lines are shown in Figure 3.

During the event, the IMF conditions were significantly disturbed, containing multiple, high magnitude transitions of the B_z component (Figure 2 (a)). B_y was strongly positive at the beginning of the event, transitioning strongly negative mid-way, then decreasing in magnitude along with B_z near the end. Although B_z is the dominant driver of the solar wind-magnetosphere dynamo, both components ultimately have a large influence on plasma convection in the ionosphere, and by a large extent, dictate its velocity.

In Figure 2 (b), it is visible by eye that the average magnitudes of both the plasma and neutral velocity exhibited a sinusoid-like evolution of an approximately similar pe-

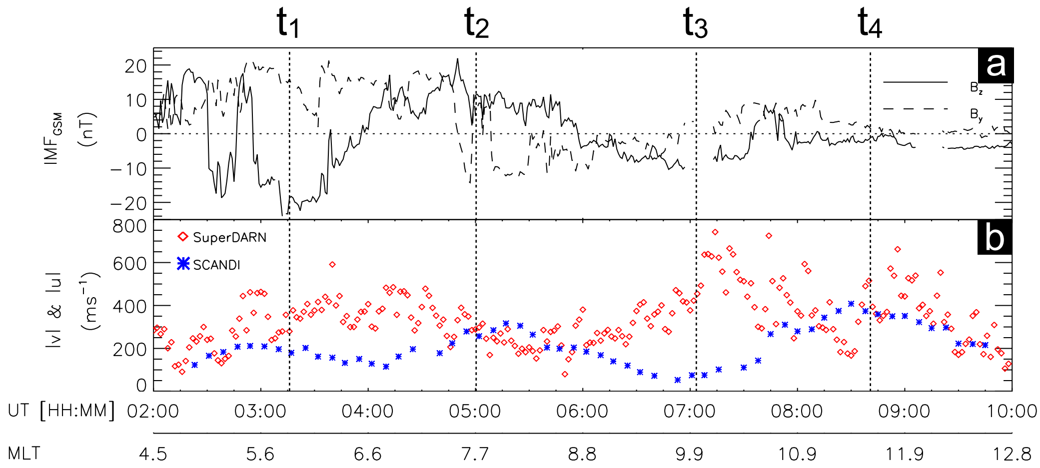

Figure 2. 8th December, 2013 event between 02:00 and 10:00 UT. The magnetic local time (MLT) of SCANDI's central zone is also shown for reference on the bottom axis. (a): IMF B_z and B_y components. (b): Spatially averaged plasma (red) and neutral (blue) velocity magnitudes over the entire SCANDI field of view, measured by SuperDARN and SCANDI respectively. The four vertical dashed lines (t_1, t_2, t_3 and t_4) indicate the times of the polar plots shown in Figure 3. The inconsistent offset between UT and MLT at a fixed point is due to the magnetic pole offset to the terrestrial spin axis, meaning certain magnetic local times are swept out faster than others.

riodicity. The temporal variability of the neutral winds was smoother than the plasma, and the latter was nearly always larger in magnitude. When the first southward B_z turning occurred just before 02:30UT, the plasma responded almost immediately and sped up. A short-lived northward turning occurred for approximately 10-15mins shortly before 03:00UT, however, this did not appear to last long enough to propagate into the plasma velocity. A typical, two cell convection pattern was formed (Figure 3 (a)) that extends equatorward enough for SCANDI to be located on the poleward side of the dawn cell. The neutrals were approximately perpendicular to plasma flow here. Upon the northward turning at 04:00UT, the plasma velocity had peaked and began to slow down (Figure 3 (b)) to a minimum at 05:30UT. Here it can be seen that the neutrals have turned completely anti-sunward, into the flow of convection across the polar cap. The subsequent period of southward B_z between approximately 06:00UT and 07:45UT resulted in the plasma accelerating once more to a maximum whilst the neutral magnitude continued to die down to a minimum (Figure 3 (c)). The neutrals at this point now mostly all

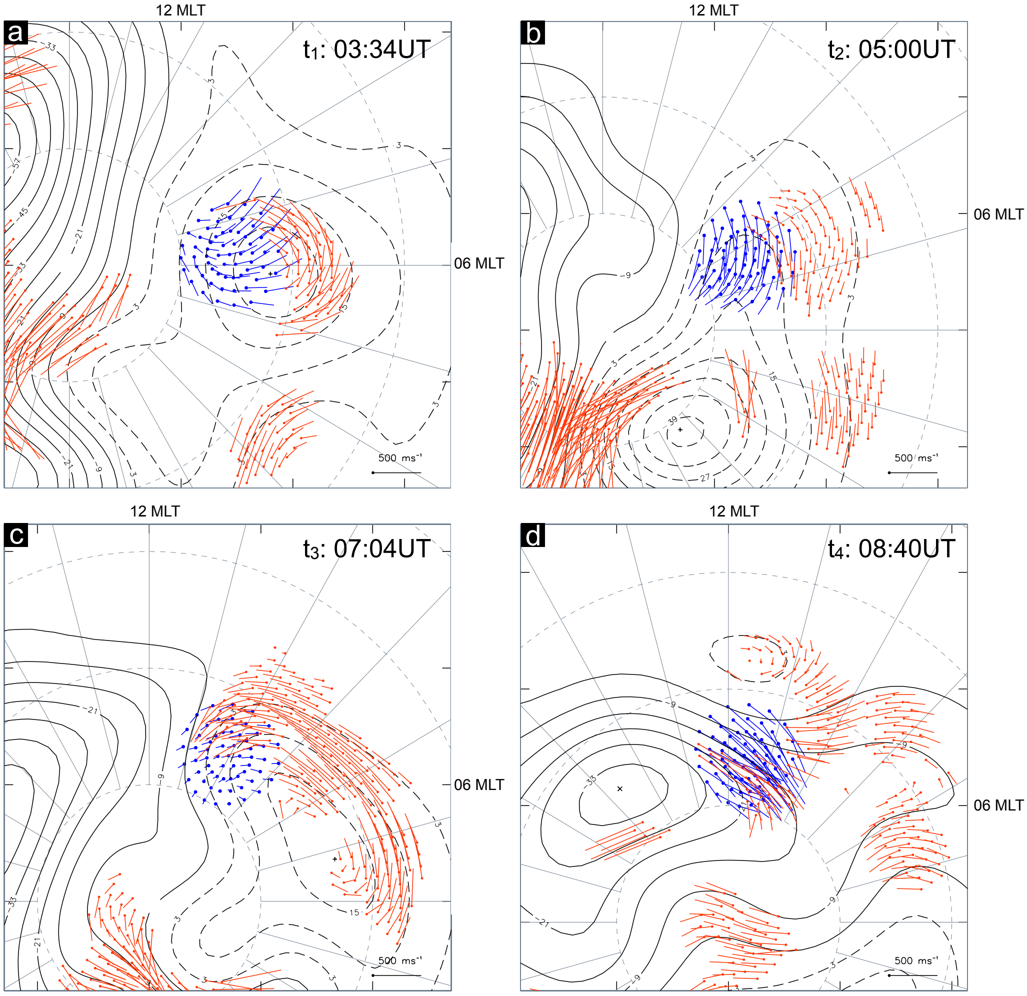

Figure 3. MLT-MLAT plots showing SuperDARN fitted model vectors in the locations of measured backscatter (red vectors) and SCANDI neutral vectors (blue) for the times indicated with dashed lines in Figure 2. Also shown is the electric potential solution to the data, with solid (dashed) contours indicating negative (positive) potential. Times shown correspond to the vertical dashed lines in Figure 2. (a) t_1: 03:34UT, (b) t_2: 05:00UT, (c) t_3: 07:04UT and (d) t_4: 08:40UT. Grey circles mark lines of constant latitude, separated by 10°.

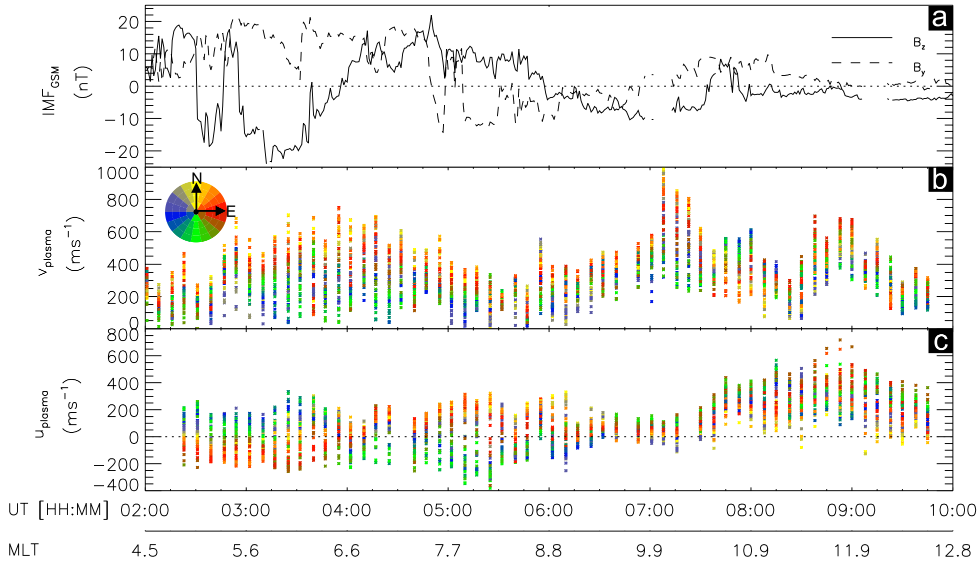

Figure 4. The same time interval as Figure 2, showing the plasma (panel (b)) and neutral wind (panel (c)) velocities in the plasma flow direction for all 61 SCANDI zones. Each data point has been coloured by SCANDI look direction in geomagnetic coordinates (a key for this colouring is shown in panel (b)).

co-propagated with the plasma. From 07:00-07:30UT, the neutral wind velocity magnitude rose sharply to match the plasma magnitude and remained comparable for around an hour (Figure 3 (d)). This was despite both the IMF B_z and B_y components being low in magnitude.

Since we are interested only in the effect of the ion-drag force on the neutrals (which will act in the plasma direction if it is faster, or opposite if slower), it is important to determine the corresponding neutral wind velocity component in the direction of the plasma (u_{plasma}). This was achieved by temporally averaging each plasma vector to the integration time of the SCANDI data, then calculating the angle between each plasma and neutral wind vector pair. By using the individual vector magnitudes in the plasma direction, corresponding to each SCANDI zone, 61 neutral and plasma velocity time series were available. These are shown for this event in Figure 4 (b) and (c), respectively. Each time series has been coloured by look direction of the zone it represents in AACGM coordinates, a visual representation of which is shown by the multi-colour circle in the top left of Figure 4 (b). The purpose of this colouring is to show groupings of zones with similar velocities, and thus distinguish spatial structure in the data. Solar wind conditions are shown again for reference in Figure 4 (a). It is these time series that were used to quantitatively determine the neutral wind lag time in each zone via cross-correlation analysis.

The plasma speeds (Figure 4 (b)) were slowest in the southern-most and fastest in the northern-most zones for the period contained firmly in the dawn sector (4.5 - 9 MLT). As the region of interest moved closer to magnetic noon, the spread of plasma velocities reduced significantly ($\sigma = 209\,\mathrm{ms}^{-1}$, $\sigma = 108\,\mathrm{ms}^{-1}$ at 04:00UT and 09:00UT respectively). For $\mathrm{u}_{\mathrm{plasma}}$ (panel c), the difference between the slowest and fastest measured velocities is more steady with developing local time. At the beginning of the event until 06:30UT, approximately half of the zones had a positive neutral wind component in the plasma direction whilst the other half opposed. At around 04:00UT however, neutrals in the eastern zones accelerated into the plasma direction (see also Figure 3 (b) for approximately the same time). This also coincides with the plasma velocity in the eastern zones being faster than in others. At 05:30, the neutral and plasma velocities are comparable. From around 06:30UT until the end of the event, nearly all of the neutral wind vectors measured by SCANDI were broadly consistent with the plasma flow. Over the entire period, plasma velocities varied by up to $800\,\mathrm{ms}^{-1}$ and neutrals up to $500\,\mathrm{ms}^{-1}$, which is evidence for significant spatial structure over the field of view observed in both parameters.

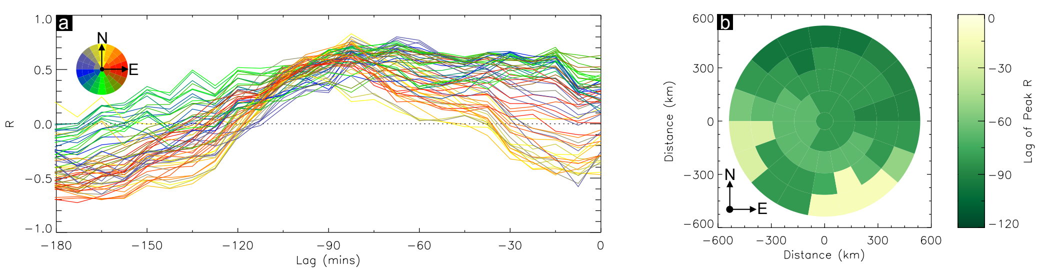

Figure 5. (a): Correlation coefficients versus lag for each time series pair, coloured by zone as in Figure 4 (b) and (c). (b): SCANDI zone configuration, coloured by the lag value corresponding to a peak in correlation coefficient (R) for each zone. Negative lag values indicate the neutral time series are shifted backwards in time.

The cross correlation was achieved by calculating a correlation coefficient for each neutral time series against a version of the corresponding plasma time series, offset by some time interval (lag). Each latter half of the u_{plasma} time series were lagged in steps equal to the SCANDI integration time to match the cadence of the time averaged data in Figure 4, backwards, to a maximum of -180 minutes. We only lag backwards as a way to extract the effects of forcing from the plasma. We consider the possibility of the neutrals maintaining the plasma flow after the solar wind driving subsides - the so called neutral wind flywheel effect - separately, in section 4, below.

The results of the cross correlation analysis are shown in Figure 5 (a) for each zone using the same directional based colours as Figure 4. A correlation coefficient (R-value) of 1 indicates perfect correlation, i.e. the compared time series peak and trough at the same time. Conversely, an R of -1 indicates perfect anti-correlation. In this study, we take the lag with the highest positive R as the lag time of the neutral wind response to changes in the plasma. The correlation curves for all zones have a similar shape, characterised by a distinct and consistent decrease in R either side of the peak at -75 minutes which is steeper on the longer lag side. This is a convincing indication that for the event in question, the neutrals lagged around 75 minutes behind changes in the plasma on average. The time lag with maximum R is shown in Figure 5 (b) for each of SCANDI's zones. The range of lags across all zones gives an indication of how the strength of ion-neutral coupling varies on mesoscale lengths. R peaks at an average lag of approximately -75 minutes for most zones, the exception being the south-eastern and westernmost zones of the SCANDI field of view.

4 Discussion

The event presented here shows distinctive forcing of the neutrals due to changes in plasma velocity. Following an extensive search for similar events, we can conclude that our event is not typical. It was postulated that in order to make the effect of changes in ion-drag forcing clearly apparent in neutral velocity data, a period of steady northward or southward IMF B_z, followed by a clear transition, was required. This should result in a step change in plasma velocity as a response. If, after this transition, B_z remained steady once more for a period of time longer than the neutral wind lag time, then a response in the neutral velocity measurements should be visible as they accelerate (or decelerate) to to the new plasma velocity. For the case of a north to south transition in

B_z for instance, we would expect a relatively fast increase in plasma velocity, followed by a gradual increase in the neutral velocity. There are however caveats to this which mean that many events meeting the transition criteria did not display an obvious neutral wind reaction to a step change in plasma velocity. Factors such as local time, latitude and the expanding-contracting polar cap (Milan, Boakes, & Hubert, 2008; Walach, Milan, Yeoman, Hubert, & Hairston, 2017) complicate issues further with respect to which region of convection was being observed. There will also be an effect from non-ion-drag forces on the measured neutral velocities from SCANDI, including the Coriolis, centrifugal, advection and viscous forces, as well as those due to strong solar pressure gradients on the dayside (Förster et al., 2008; Lühr, Rentz, Ritter, Liu, & Häusler, 2007; Thayer & Killeen, 1993). The latter imparts both a seasonal and universal time dependence, which has a known impact statistically (Billett, Grocott, Wild, Walach, & Kosch, 2018), but is likely to be eclipsed by ion-drag forces during geomagnetically-active events. As the event began on the nightside, there was also a potential influence from any substorm activity (Weimer, 2001), but significantly less pressure forces on the neutrals because of smaller temperature gradients compared to the dayside (Jacchia, 1965). With all these in mind, it is thus important to justify why the event described in particular so ideally demonstrated the influence of ion-drag on the neutrals.

Since the event occurred mainly in the dawn sector and at an AACGM latitude of approximately 75.8°, the plasma flow within the region of interest could be either the sunward return flow or anti-sunward flow across the geomagnetic polar cap, depending on the equatorward extent of the large-scale Dungey cycle convection pattern. Indeed, this is apparent in Figure 3 which shows that SCANDI was always located on the poleward or sunward edge of the dawn cell in the region of anti-sunward flow. The plasma velocity differences between the latitudinally separated northern and southern most zones, seen at the beginning of the event in Figure 4 (b), can be attributed to observing different regions of the poleward side of the convection dawn cell (e.g. in Figure 3 (a)). Overall, this means any significant velocity changes seen in the plasma data were likely due to variations in solar wind driving conditions and not due to the radars moving into a different region of convection over time. This however does not hold completely true nearer the end of the event; after a decrease in plasma velocity between 0715 and 0830UT, there was another substantial increase, even though IMF magnitudes were considerably weaker than before (Figure 3 (d)). We propose that this acceleration was due to the neutral wind flywheel effect (Lyons, Killeen, & Walterscheid, 1985), i.e. neutrals with lingering inertia applying an accelerating force to the plasma.

In the same vein as the neutrals needing time to fully accelerate due to ion-drag, they will also take time to decelerate assuming there was no additional forcing from the plasma. However, this was not what we saw for u_{plasma} nearer the end of the interval shown in Figure 4. Right at the point where the neutrals overtook the plasma in velocity (~08:30UT), the plasma reaches a minimum velocity and then accelerates back up to the velocity of the neutrals quite sharply. The neutrals speed up slightly after the plasma slows, and then remain fairly steady. Most of this sustained neutral wind momentum is likely due to inertia of neutral particles themselves, as solar pressure gradients do not change substantially over the short spatial regions considered here. Additional non-ion drag forces, such as dayside auroral heating, may have also contributed to continued high velocities. The neutrals now pull the plasma with it (instead of the other way around; see Figure 3 (d)) and generate electric fields in a similar fashion to the low latitude dynamo (Richmond, 1989). Figure 3 (d) also shows that the plasma was significantly disturbed elsewhere on the dayside during this period, indicating that flywheel forcing might not have been limited to just the observing volume of SCANDI.

As mentioned previously, there are many other forces besides ion-drag that act upon the neutral winds. By resolving the neutral velocity into the direction of the plasma, we attempt to isolate only the influence of ion-drag. However, any force which happened to also act in plasma flow direction (or directly opposite) would also translate into the u_{plasma} component. For example, during the times shown in Figure 3, SCANDI was mostly located in the region of anti-sunward convection over the polar cap. Ion-drag was therefore acting in this direction, but so was the pressure gradient forces brought about by increased dayside heating. This could account partly for the u_{plasma} increase from around 0800UT in 4 (c) (and also the flywheel forcing mentioned prior), but does not explain the turning of the neutrals anti-sunward between Figure 3 (a) and (b). This is because during the northern hemispheric winter, the solar pressure gradient is not steep around dawn (Wallis & Budzinski, 1981).

When considering which lag gives the peak R values for each zone (Figure 5 (b)), it is important to associate a zone with its corresponding correlation curve in Figure 5 (a). The south-eastern and westernmost zones had considerably different 'best' lags than the majority of other zones, although their curves similarly peaked at a lag of around -75 minutes, in line with the others. This illustrates well a potential caveat of the cross-correlation technique for determining neutral wind lag times. The peaks and troughs for the neutral and plasma velocities were fairly distinct (see Figure 4 (b) and (c)), yielding a well-defined peak in R at around -75 minutes. However, there are some local peaks in R observed at other lags (e.g. at around -15 minutes for the southern zones in green).

If these zones with slightly higher correlation peaks at earlier lags are ignored, the neutral wind lag time is found to vary between extremes of -67 and -97 minutes. This result is consistent with studies by Joshi et al. (2015) and Heelis, McEwen, and Guo (2002), whilst falling within the range of lags calculated by other studies (Baron & Wand, 1983; Killeen et al., 1984; Kosch et al., 2001). It is interesting that there is no discreet jump in lag shown in figure 5 (b) (apart from those previously mentioned), but a gradual change across the 1000 km field of view. This indicates that changes in the strength of coupling between the plasma and neutrals can be significant on mesoscale lengths of a few hundred kilometers horizontally, rather than lesser distances (i.e. in neighbouring zones). Ultimately, it means that the rate and amount of energy transfer between the plasma and neutrals will vary substantially across these spatial scales, as neutrals in some regions will re-orientate into the plasma direction more quickly than in others.

Lag times appear to be shorter for the south-western zones, whilst east-north-eastern zones are delayed longer. However, the potential variability of lags with local time, and thus universal time, is not well understood and could affect the results shown here. On average, Svalbard is poleward of the auroral oval. However, a likely reason for the shorter lags in some of the southern zones is the influence of auroral ionisation as the area of interest moved to the dayside (where the auroral oval is typically at higher latitudes than on the nightside). As studied by Conde et al. (2018) and Zou et al. (2018), the drastic increase in ion density introduced by precipitation will enhance the neutral-ion collision frequency, which in turn strengthens ion-drag. Future work in this area will examine ion-neutral coupling during active auroral periods, in conjunction with a measure of thermospheric ionisation (such as that determined from the EISCAT radar network). In addition, the positioning of Svalbard allows for the unique opportunity to make observations in the dayside cusp region where the convection electric fields are quickly influenced by dayside reconnection.

5 Summary

We have identified an event which shows clear forcing of the thermospheric neutral wind from ionospheric convection above Svalbard. A cross correlation analysis was performed using spatially resolved SuperDARN and SCANDI data to quantitatively determine the timescale upon which ion-drag fully accelerates the neutrals into the direction of plasma motion, and if there was any variation of this lag over a range of approximately 1000 km. It was found that for this event which contained multiple, distinct IMF B_z transitions of high magnitude, the neutral wind response to enhancements in plasma convection was significant and readily apparent. The cross correlation analysis revealed the following:

- Over the entire SCANDI field of view, the average lag time of the neutrals for a high activity event on the dawn side was approximately 75 minutes.
- On smaller spatial scales within the SCANDI field of view, the lag time of the neutrals varied between extremes of 67 and 97 minutes depending on location. Shorter lags occurred to the south of SCANDI (equatorward), while longer lags occurred to the north (poleward).

In addition to these points, we observe flywheel forcing of the ionospheric plasma once the neutral wind velocity begins to overtake in velocity. As ion-drag cannot accelerate the neutrals past the plasma speed, residual neutral wind inertia resulted in an induced neutral wind dynamo electric field above Svalbard for a short period of time.

Our results agree with previous studies, and provide new insights to the role of ion-drag forcing on considerably smaller spatial scales. A 30 minute difference has been observed in neutral wind lag times for regions of space less than 1000 km apart, induced by the significant discord between neutral and plasma motion on those scales (which was made especially apparent due to strong and variable IMF driving forces). This means that different regions of the thermosphere respond to changes in the ionosphere at comparatively different rates, which would change the amount of Joule heating deposited across these spatial scales significantly. Additionally, non ion-drag forces, which contribute to mesoscale neutral wind variations, also potentially affect the lag of the neutrals. With regards to how exactly the thermosphere and ionosphere are coupled on the small spatial scales shown in this study, more work is needed to quantify the effects of ionisation due to increased precipitation, local time, season and other geomagnetic conditions.

Acknowledgments

The authors acknowledge the use of data from SuperDARN, an international project made possible by the national funding agencies of Australia, Canada, China, France, Japan, South Africa, the United Kingdom and the United States of America. The UCL Scanning Doppler Imager (SCANDI) is maintained thanks to Dr Ian McWhirter, whose efforts are gratefully acknowledged. The SuperDARN convection modelling procedure was performed using the Radar Software Toolkit version 4.1 (https://github.com/SuperDARN/rst). Quick-look SuperDARN data plots can be viewed online at http://vt.superdarn.org/tiki-index.php?page=ASCIIData. OMNI solar wind data can be viewed and downloaded at https://omniweb.gsfc.nasa.gov/. During this study, D.D.B was supported by Lancaster University. A.G, A.L.A, A.M.R and M.-T.W were supported by NERC grant NE/P001556/1.

References

Aruliah, A., Griffin, E., Yiu, H.-C., McWhirter, I., & Charalambous, A. (2010). SCANDI–an all-sky Doppler imager for studies of thermospheric spatial structure. *Annales Geophysicae (09927689)*, *28*(2).

Baron, M. J., & Wand, R. H. (1983). F region ion temperature enhancements resulting from Joule heating. *Journal of Geophysical Research: Space Physics*, *88*(A5), 4114–4118.

Billett, D., Grocott, A., Wild, J., Walach, M.-T., & Kosch, M. (2018). Diurnal variations in global Joule heating morphology and magnitude due to neutral winds. *Journal of Geophysical Research: Space Physics*, *123*(3), 2398–2411.

Chisham, G., Lester, M., Milan, S. E., Freeman, M., Bristow, W., Grocott, A., ... others (2007). A decade of the super dual auroral radar network (SuperDARN): Scientific achievements, new techniques and future directions. *Surveys in Geophysics*, *28*(1), 33–109.

Conde, M., Bristow, W., Hampton, D., & Elliott, J. (2018). Multi-instrument studies of thermospheric weather above Alaska. *Journal of Geophysical Research: Space Physics*.

Conde, M., & Smith, R. (1997). Phase compensation of a separation scanned, all-sky imaging Fabry-Perot spectrometer for auroral studies. *Applied Pptics*, *36*(22), 5441–5450.

Conde, M., & Smith, R. (1998). Spatial structure in the thermospheric horizontal wind above Poker Flat, Alaska, during solar minimum. *Journal of Geophysical Research: Space Physics*, *103*(A5), 9449–9471.

Cousins, E., & Shepherd, S. (2010). A dynamical model of high-latitude convection derived from SuperDARN plasma drift measurements. *Journal of Geophysical Research: Space Physics*, *115*(A12).

Cowley, S., & Lockwood, M. (1992). Excitation and decay of solar wind-driven flows in the magnetosphere-ionosphere system. In *Annales geophysicae* (Vol. 10, pp. 103–115).

Drob, D. P., Emmert, J. T., Meriwether, J. W., Makela, J. J., Doornbos, E., Conde, M., … others (2015). An update to the horizontal wind model (hwm): The quiet time thermosphere. *Earth and Space Science*, *2*(7), 301–319.

Dungey, J. W. (1961). Interplanetary magnetic field and the auroral zones. *Physical Review Letters*, *6*(2), 47.

Eather, R., & Mende, S. (1971). Airborne observations of auroral precipitation patterns. *Journal of Geophysical Research*, *76*(7), 1746–1755.

Emmert, J., Hernandez, G., Jarvis, M., Niciejewski, R., Sipler, D., & Vennerstrom, S. (2006). Climatologies of nighttime upper thermospheric winds measured by ground-based Fabry-Perot interferometers during geomagnetically quiet conditions: 2. high-latitude circulation and interplanetary magnetic field dependence. *Journal of Geophysical Research: Space Physics*, *111*(A12).

Förster, M., Rentz, S., Köhler, W., Liu, H., & Haaland, S. (2008). IMF dependence of high-latitude thermospheric wind pattern derived from CHAMP crass-track measurements. In *Annales geophysicae: atmospheres, hydrospheres and space sciences* (Vol. 26, p. 1581).

Grocott, A., & Milan, S. E. (2014). The influence of IMF clock angle timescales on the morphology of ionospheric convection. *Journal of Geophysical Research: Space Physics*, *119*(7), 5861–5876.

Heelis, R., McEwen, D., & Guo, W. (2002). Ion and neutral motions observed in the winter polar upper atmosphere. *Journal of Geophysical Research: Space Physics*, *107*(A12).

Jacchia, L. G. (1965). New static models of the thermosphere and exosphere with empirical temperature profiles. *SAO special report*, *313*.

Joshi, P., Baker, J., Ruohoniemi, J., Makela, J., Fisher, D., Harding, B., ... Thomas, E. (2015). Observations of storm time midlatitude ion-neutral coupling using SuperDARN radars and nation Fabry-Perot interferometers. *Journal of Geophysical Research: Space Physics*, *120*(10), 8989–9003.

Killeen, T., Hays, P., Carignan, G., Heelis, R., Hanson, W., Spencer, N., & Brace, L. (1984). Ion-neutral coupling in the high-latitude F region: Evaluation of ion heating terms from Dynamics Explorer 2. *Journal of Geophysical Research: Space Physics*, *89*(A9), 7495–7508.

Kohl, H., & King, J. (1967). Atmospheric winds between 100 and 700 km and their effects on the ionosphere. *Journal of Atmospheric and Terrestrial Physics*, *29*(9), 1045–1062.

Kosch, M., Cierpka, K., Rietveld, M., Hagfors, T., & Schlegel, K. (2001). High-latitude ground-based observations of the thermospheric ion-drag time constant. *Geophysical Research Letters*, *28*(7), 1395–1398.

Kurihara, J., Oyama, S., Nozawa, S., Tsuda, T., Fujii, R., Ogawa, Y., ... others (2009). Temperature enhancements and vertical winds in the lower thermosphere associated with auroral heating during the DELTA campaign. *Journal of Geophysical Research: Space Physics*, *114*(A12).

Lühr, H., Rentz, S., Ritter, P., Liu, H., & Häusler, K. (2007). Average thermospheric wind patterns over the polar regions, as observed by CHAMP. *Annales Geophysicae*, *25*(5), 1093–1101.

Lyons, L., Killeen, T., & Walterscheid, R. (1985). The neutral wind flywheel as a source of quiet-time, polar-cap currents. *Geophysical Research Letters*, *12*(2), 101–104.

Milan, S., Boakes, P., & Hubert, B. (2008). Response of the expanding/contracting polar cap to weak and strong solar wind driving: Implications for substorm onset. *Journal of Geophysical Research: Space Physics*, *113*(A9).

Murr, D., & Hughes, W. (2001). Reconfiguration timescales of ionospheric convection. *Geophysical Research Letters*, *28*(11), 2145–2148.

Richmond, A. (1989). Modeling the ionosphere wind dynamo: A review. *Pure and Applied Geophysics*, *131*(3), 413–435.

Richmond, A., Lathuillere, C., & Vennerstrøm, S. (2003). Winds in the high-latitude lower thermosphere: Dependence on the interplanetary magnetic field. *Journal of Geophysical Research: Space Physics*, *108*(A2).

Richmond, A., Ridley, E., & Roble, R. (1992). A thermosphere/ionosphere general circulation model with coupled electrodynamics. *Geophysical Research Letters*, *19*(6), 601–604.

Ruohoniemi, J., & Baker, K. (1998). Large-scale imaging of high-latitude convection with super dual auroral radar network HF radar observations. *Journal of Geophysical Research: Space Physics*, *103*(A9), 20797–20811.

Ruohoniemi, J., & Greenwald, R. (1996). Statistical patterns of high-latitude convection obtained from goose bay HF radar observations. *Journal of Geophysical Research: Space Physics*, *101*(A10), 21743–21763.

Ruohoniemi, J., & Greenwald, R. (2005). Dependencies of high-latitude plasma convection: Consideration of interplanetary magnetic field, seasonal, and universal time factors in statistical patterns. *Journal of Geophysical Research: Space Physics*, *110*(A9).

Shepherd, S. (2014). Altitude-adjusted corrected geomagnetic coordinates: Definition and functional approximations. *Journal of Geophysical Research: Space Physics*, *119*(9), 7501–7521.

Thayer, J. P., & Killeen, T. (1993). A kinematic analysis of the high-latitude thermospheric neutral circulation pattern. *Journal of Geophysical Research: Space Physics*, *98*(A7), 11549–11565.

Thomas, E. G., & Shepherd, S. (2018). Statistical patterns of ionospheric convection derived from mid-latitude, high-latitude, and polar SuperDARN HF radar observations. *Journal of Geophysical Research: Space Physics*, *123*(4), 3196–3216.

Titheridge, J. (1995). Winds in the ionosphere A review. *Journal of Atmospheric and Terrestrial Physics*, *57*(14), 1681–1714.

Walach, M.-T., Milan, S. E., Yeoman, T., Hubert, B., & Hairston, M. (2017). Testing nowcasts of the ionospheric convection from the expanding and contracting polar cap model. *Space Weather*, *15*(4), 623–636.

Wallis, D., & Budzinski, E. E. (1981). Empirical models of height integrated conductivities. *Journal of Geophysical Research: Space Physics*, *86*(A1), 125–137.

Weimer, D. (2001). An improved model of ionospheric electric potentials including substorm perturbations and application to the geospace environment modeling November 24, 1996, event. *Journal of Geophysical Research: Space Physics*, *106*(A1), 407–416.

Weimer, D. (2005). Improved ionospheric electrodynamic models and application to calculating Joule heating rates. *Journal of Geophysical Research: Space Physics*, *110*(A5).

Zou, Y., Nishimura, Y., Lyons, L., Conde, M., Varney, R., Angelopoulos, V., & Mende, S. (2018). Mesoscale F region neutral winds associated with quasi-steady and transient nightside auroral forms. *Journal of Geophysical Research: Space Physics*.